Available online at www.sciencedirect.com
SCIENCE DIRECT®
PERGAMON
International Journal of Heat and Mass Transfer 46 (2003) 2587–2601
International Journal of HEAT and MASS TRANSFER
www.elsevier.com/locate/ijhmt

Active nucleation site density in boiling systems

Takashi Hibiki [a,b], Mamoru Ishii [b,*]

[a] Research Reactor Institute, Kyoto University, Noda, Kumatori, Sennan, Osaka 590-0494, Japan
[b] School of Nuclear Engineering, Purdue University, 400 Central Drive, West Lafayette, IN 47907-2017, USA

Received 30 August 2002; received in revised form 24 December 2002

Abstract

Realizing the significance of the active nucleation site density as an important parameter for predicting the interfacial area concentration in a two-fluid model formulation, the active nucleation site density has been modeled mechanistically by knowledge of the size and cone angle distributions of cavities that are actually present on the surface. The newly developed model has been validated by various active nucleation site density data taken in pool boiling and convective flow boiling systems. The newly developed model clearly shows that the active nucleation site density is a function of the critical cavity size and the contact angle, and the model can explain the dependence of the active nucleation site density on the wall superheat reported by various investigators. The newly developed model can give fairly good predictions over rather wide range of the flow conditions (0 kg/m^2 s $\leqslant$ mass velocity $\leqslant$ 886 kg/m^2 s; 0.101 MPa $\leqslant$ pressure $\leqslant$ 19.8 MPa; 5° $\leqslant$ contact angle $\leqslant$ 90°; 1.00×10^4 sites/m^2 $\leqslant$ active nucleation site density $\leqslant$ 1.51×10^{10} sites/m^2).

Keywords: Active nucleation site; Interfacial area transport; Two-fluid model; Subcooled boiling flow; Pool boiling; Contact angle

1. Introduction

In the past 25 years, significant developments in the two-phase flow formulation have been accomplished by the introduction of the drift flux model and the two-fluid model. In the present state-of-the-art, the two-fluid model is the most detailed and accurate macroscopic formulation of the thermo-fluid dynamics of two-phase systems. In the two-fluid model, the field equations are expressed by the six conservation equations consisting of mass, momentum and energy equations for each phase. Since these field equations are obtained from an appropriate averaging of local instantaneous balance equations, the phasic interaction term appears in each of the averaged balance equation. These terms represent the mass, momentum and energy transfers through the interface between the phases. The existence of the interfacial transfer terms is one of the most important characteristics of the two-fluid model formulation. These terms determine the rate of phase changes and the degree of mechanical and thermal non-equilibrium between phases, thus they are the essential closure relations which should be modeled accurately. However, because of considerable difficulties in terms of measurements and modeling, reliable and accurate closure relations for the interfacial transfer terms are not fully developed [1].

In relation to the modeling of the interfacial transfer terms, the concept of the interfacial area transport equation has recently been proposed to develop the constitutive relation on the interfacial area concentration [2]. The interfacial area concentration change can basically be characterized by the variation of the particle number density due to coalescence and breakup of bubbles. The interfacial area transport equation can be derived by considering the fluid particle number density transport equation analogous to Boltzmann's transport equation [2]. The interfacial area transport equation can replace the traditional flow regime maps and regime transition criteria. The changes in the two-phase flow structure can be predicted mechanistically by introducing the interfacial area transport equation. The effects of the boundary conditions and flow development are

* Corresponding author. Tel.: +1-765-494-4587; fax: +1-765-494-9570.
E-mail addresses: hibiki@rri.kyoto-u.ac.jp (T. Hibiki), ishii@ecn.purdue.edu (M. Ishii).

0017-9310/03/$ - see front matter
doi:10.1016/S0017-9310(03)00031-0

Nomenclature

A	measuring area
A_C	cross-sectional area of boiling channel
a_i	interfacial area concentration
C	parameter
C_1	parameter
C_{pf}	liquid specific heat
C_{pw}	wall specific heat
D_c	critical cavity diameter
D_d	bubble departure diameter
D_{dF}	bubble departure diameter calculated by Fritz equation
f	bubble generation frequency from active sites
$f(r)$	function of r
$f(\beta)$	function of β
$f'(\beta)$	function of β
$f(\rho^*)$	function of ρ^*
$f(\rho^+)$	function of ρ^+
G	mass velocity
g	gravitational acceleration
i_{fg}	latent heat
K	parameter
K_1	parameter
m	exponent
N_n	active nucleation site density
N_n^+	non-dimensional active nucleation site density
$\overline{N_n}$	average cavity density
N_{nc}	active nucleation site density in forced convective boiling
N_{np}	active nucleation site density in pool boiling
N_n^*	non-dimensional active nucleation site density
N_{np}^*	non-dimensional active nucleation site density in pool boiling
$N_{n,H-I}^*$	non-dimensional active nucleation site density
$N_{n,Y-K}^*$	non-dimensional active nucleation site density
n_b	bubble number density
n_c^r	number of cavity in a certain cavity radius range
n_c^β	number of cavity in a certain half of cone angle
P	pressure
P_f	liquid pressure
Pr	Prandtl number
q_w	wall heat flux
R_a	arithmetic average roughness
R_c	critical cavity radius
R_c^*	non-dimensional critical cavity radius
R_c^+	non-dimensional critical cavity radius
R_m	maximum cavity size derived by Yang and Kim's model
R_{max}	maximum cavity size
R_s	structure upper limit of cavity radius
r	cavity radius
S	suppression factor
s	standard deviation
T_0	bulk liquid temperature at practical boiling incipience point
T_f	bulk liquid temperature
T_g	gas temperature
T_{sat}	saturation temperature
T_w	wall temperature
t	time
v_{bz}	average bubble velocity
v_{iz}	interfacial velocity
z	axial coordinate

Greek symbols

α	void fraction
β	half of cone angle
$\bar{\beta}$	mean half of cone angle
γ	surface–liquid interaction parameter
Δr	certain range of cavity radius
ΔT_e	effective wall superheat
ΔT_{ONB}	wall superheat at onset of nucleate boiling
ΔT_{sat}	gas superheat
$\Delta T_{sub,in}$	inlet subcooling
ΔT_W	wall superheat
$\Delta\beta$	certain range of half of cone angle
$\Delta\rho$	density difference
Θ	dimensionless surface roughness parameter
θ	contact angle
κ_f	liquid thermal conductivity
κ_W	wall thermal conductivity
λ	statistical parameter
λ'	statistical parameter
μ	statistical parameter
μ_f	liquid viscosity
ξ_H	heated perimeter
ρ_f	liquid density
ρ_g	vapor density
ρ_W	wall density
ρ^*	non-dimensional density difference
ρ^+	non-dimensional density difference
σ	interfacial tension
Φ_{BB}	interfacial area concentration source rate due to bubble breakup
Φ_{BC}	interfacial area concentration sink rate due to bubble coalescence
Φ_{BE}	interfacial area concentration change rate due to bubble expansion or shrinkage

Φ_{HE}	interfacial area concentration rate source due to heterogeneous bubble nucleation
Φ_{PC}	interfacial area concentration sink rate due to condensation
Φ_{WN}	interfacial area concentration source rate due to bubble nucleation from active cavities
ϕ_{BB}	bubble source rate due to bubble breakup
ϕ_{BC}	bubble sink rate due to bubble coalescence
ϕ_{BN}	bubble nucleation rate in bulk liquid
ϕ_{HE}	heterogeneous bubble nucleation rate
ϕ_{HO}	homogeneous bubble nucleation rate
ϕ_{PC}	bubble sink rate due to condensation
ϕ_{WN}	bubble nucleation rate from active cavities
$\phi(r)$	function of r
$\phi(\theta)$	function of θ
$\phi'(\theta)$	function of θ

Subscripts

calc.	calculated value
meas.	measured value

efficiently modeled by this transport equation. Such a capability does not exist in the current state-of-the-art nuclear thermal–hydraulic system analysis codes like RELAP5, TRAC and CATHARE. Thus, a successful development of the interfacial area transport equation can make a quantum improvement in the two-fluid model formulation and the prediction accuracy of the system codes.

In order to develop the interfacial area transport equation, considerable efforts have recently been made (1) to formulate the interfacial area transport equation, (2) to develop measurement techniques for local flow parameters, (3) to construct data base of axial development of local flow parameters, (4) to model sink and source terms in the interfacial area transport equation, and (5) to improve thermal–hydraulic system analysis codes by implementing the interfacial area transport equation. The present status of the development of the interfacial area transport equation was extensively reviewed in the previous papers [3,4]. In the first stage of the development of the interfacial area transport equation, adiabatic flow was the focus, and the interfacial area transport equation for the adiabatic flow was developed successfully by modeling sink and source terms of the interfacial area concentration due to bubble coalescence and breakup. The hydrodynamic effects on the interfacial area transport have been revealed through a series of the studies. It has been demonstrated that the interfacial area transport equation can give a good prediction providing the initial bubble size is given. In the next stage, subcooled boiling flow was the focus, and a preliminary local measurement for interfacial area concentration was initiated for subcooled boiling water flow in an internally heated annulus [5]. A modeling of source and sink terms due to phase change will be required to develop the interfacial area transport equation in boiling flow. However, most critical subject to finalize the interfacial area transport equation in boiling flow would be to model the initial and boundary conditions, which will be described as a function of an active nucleation site density, a bubble generation frequency, and a bubble departure size. Realizing the significance of the initial and boundary conditions for predicting the interfacial area in a forced convective nucleate boiling, Kocamustafaogullari and Ishii [6] performed (i) the formulation of the bubble number density in terms of the differential balance equation which took into account various parameters such as the bulk liquid nucleation, the wall cavity nucleation and the bubble collapse rates through the source and sink terms, (ii) the discussion on the numerical importance of these parameters in the subcooled, as well as the saturated nucleate boiling region, and (iii) the development of an empirical correlation for the heated surface cavity nucleation rate which could be used as a constitutive equation in the bubble number density transport equation. When Kocamustafaogullari and Ishii performed the research on the active nucleation site density, the knowledge on boiling and, in particular, on surface nucleation characteristics were not unfortunately sufficient for building up a valid general model to correlate the active nucleation site density. Then, they decided to correlate the existing experimental data by means of parameteric study. Recently, some important observations were reported by several investigators [7–15]. Based on the recent observations, this study will aim at developing a new theoretical model to correlate the active nucleation site density.

2. One-dimensional interfacial area transport equation

Kocamustafaogullari and Ishii derived the one-dimensional transport equation for predicting the average bubble number density by considering a boiling channel with a constant cross-sectional area as [6]

$$\frac{\partial n_b}{\partial t} + \frac{\partial}{\partial z}(n_b v_{bz}) = \phi_{BN} + \phi_{WN} + \phi_{BB} - \phi_{BC} - \phi_{PC}, \quad (1)$$

where n_b, t, v_{bz}, ϕ_{BN}, ϕ_{WN}, ϕ_{BB}, ϕ_{BC} and ϕ_{PC} are the bubble number density, the time, the average bubble velocity, the bubble nucleation rate in the bulk liquid, the bubble nucleation rate from active cavities, the

bubble source rate due to bubble breakup, the bubble sink rate due to bubble coalescence, and the bubble sink rate due to condensation, respectively.

In general, bubble nucleation rate in the bulk liquid may be either of the homogeneous and heterogeneous bubble nucleation rates denoted by ϕ_{HO} and ϕ_{HE}, respectively. The homogeneous nucleation can generally be discounted as a main mechanism for bubble formation in a heated channel [6]. Thus, the bubble nucleation rate in the bulk liquid can be approximated to be the heterogeneous nucleation rate, namely $\phi_{BN} \approx \phi_{HE}$.

In a system with a heat addition, bubbles form at cavities on the heated surface known as nucleation sites. The bubble nucleation rate from active cavities can be expressed as

$$\phi_{WN} = \frac{N_n f \xi_H}{A_C}, \tag{2}$$

where N_n, f, ξ_H and A_C are the active nucleation site density, the bubble generation frequency from the active sites, the heated perimeter and the cross-sectional area of the boiling channel, respectively.

To derive the relationship between the bubble nucleation rate from active cavities and the bubble sink rate due to condensation, Kocamustafaogullari and Ishii assumed that the rate of evaporation at the surface would be proportional to the total heat flux minus the single phase convective heat flux, whereas the rate of net vapor formation would be proportional to the amount of energy that was used to increase vapor flow. Thus, the bubble sink rate due to condensation can be expressed as [6]

$$\phi_{PC} = \frac{T_{sat} - T_f}{T_{sat} - T_0}\phi_{WN}, \quad \text{for } T_0 \leqslant T_f \leqslant T_{sat}, \tag{3}$$

where T_{sat}, T_f, and T_0 are the saturation temperature, the bulk liquid temperature, and the bulk liquid temperature at the practical boiling incipience point, respectively.

The bubble source rate due to bubble breakup and the bubble sink rate due to bubble coalescence were modeled in the previous papers [1,3,4]. Combining the sink and source terms, the bubble number density transport equation can be expressed as

$$\frac{\partial n_b}{\partial t} + \frac{\partial}{\partial z}(n_b v_{bz}) = \left(\frac{T_f - T_0}{T_{sat} - T_0}\right)\left(\frac{N_n f \xi_H}{A_C}\right) + \phi_{HE} + \phi_{BB} - \phi_{BC}. \tag{4}$$

In a similar way, the interfacial area transport equation can also be expressed as

$$\frac{\partial a_i}{\partial t} + \frac{\partial}{\partial z}(a_i v_{iz}) = \Phi_{HE} + \Phi_{WE} + \Phi_{BB} + \Phi_{BE} - \Phi_{BC} - \Phi_{PC}, \tag{5}$$

where a_i, v_{iz}, Φ_{HE}, Φ_{WE}, Φ_{BB}, Φ_{BC}, and Φ_{PC} are the interfacial area concentration, the interfacial velocity, the interfacial area concentration source rate due to the bulk liquid boiling, the interfacial area concentration source rate due to the bubble nucleation from active cavities, the interfacial area concentration source rate due to bubble breakup, the interfacial area concentration sink rate due to bubble coalescence, and the interfacial area concentration sink rate due to condensation, respectively. Φ_{BE} is the interfacial area concentration change rate due to bubble expansion or shrinkage caused by pressure change along the flow channel given by

$$\Phi_{BE} = \left(\frac{2a_i}{3\alpha}\right)\left\{\frac{\partial \alpha}{\partial t} + \frac{\partial}{\partial z}(\alpha v_i)\right\}, \tag{6}$$

where α is the void fraction. The interfacial area concentration source rate due to the bubble nucleation from active cavities, Φ_{WE}, is expressed as a function of the active nucleation site density. Realizing the significance of the active nucleation site density as an important parameter in the interfacial area transport equation, a theoretical modeling of the active nucleation site density will be performed in what follows.

3. Some recent correlations for predicting active nucleation site density

In what follows, some recent correlations for predicting the active nucleation site density are briefly summarized.

3.1. Kocamustafaogullari and Ishii's model (1983)

Kocamustafaogullari and Ishii correlated existing active nucleation site density data by means of parametric study [6]. They assumed that the active nucleation site density in pool boiling, N_{np}, was influenced by both the surface conditions and the thermo-physical properties of the fluid, and developed the following correlation based on the water data.

$$N^*_{np} = f(\rho^*)R^{*-4.4}_c, \tag{7}$$

where $N^*_{np} \equiv N_{pn}D^2_d$, $f(\rho^*) = 2.157 \times 10^{-7}\rho^{*-3.2}(1 + 0.0049\rho^*)^{4.13}$, $\rho^* \equiv (\Delta\rho/\rho_g)$, and $R^*_c \equiv (R_c/(D_d/2))$. Kocamustafaogullari and Ishii gave the bubble departure diameter, D_d, by modifying the correltion of the bubble departure diameter, D_{dF}, proposed by Fritz as

$$D_d = 0.0012\rho^{*0.9}D_{dF} \quad \text{where } D_{dF} = 0.0148\theta\sqrt{\frac{2\sigma}{g\Delta\rho}}$$

or

$$D_d = 2.5 \times 10^{-5}\rho^{*0.9}\theta\sqrt{\frac{\sigma}{g\Delta\rho}}, \tag{8}$$

where σ, g, $\Delta\rho$, and θ are the surface tension, the gravitational acceleration, the density difference, and the contact angle, respectively. The minimum cavity size, R_c, can be related to the gas superheat, $\Delta T_{sat}(\equiv T_g - T_{sat})$, as:

$$R_c = \frac{2\sigma\{1 + (\rho_g/\rho_f)\}/P_f}{\exp\{i_{fg}(T_g - T_{sat})/(RT_gT_{sat})\} - 1}, \tag{9}$$

where ρ_g, ρ_f, P_f, i_{fg}, and R are the gas density, the liquid density, the liquid pressure, the latent heat and the gas constant, respectively. For $\rho_g \ll \rho_f$ and $i_{fg}(T_g - T_{sat})/(RT_gT_{sat}) \ll 1$, Eq. (9) is simplified to

$$R_c \approx \frac{2\sigma T_{sat}}{\rho_g i_{fg}\Delta T_{sat}}. \tag{10}$$

It should be noted here that for the pool boiling the approximation $\Delta T_{sat} \approx T_w(\equiv T_w - T_{sat})$, where T_w is the wall temperature, is used in Eq. (9).

Taking account of the difference between the effective liquid superheat, ΔT_e, and the wall superheat and the mechanistic similarity between pool and convective boiling, Kocamustafaogullari and Ishii postulated that the active nucleation site density correlation developed for pool boiling, Eq. (7), could be used also in the forced convective system by using an effective superheat, ΔT_e, rather than the actual wall superheat, ΔT_w. Here, the effective superheat is given by Eq. (11).

$$\Delta T_e = S\Delta T_w, \tag{11}$$

where S is the suppression factor. Thus, Kocamustafaogullari and Ishii expressed the dimensionless active nucleation site density, N_{nc}, in the convective system as

$$N^*_{nc} = f(\rho^*)R^{*-4.4}_c. \tag{12}$$

Kocamustafaogullari and Ishii evaluated their correlation with various existing data, and concluded that the correlation gave fairly good predictions.

3.2. Yang and Kim's model (1988)

Yang and Kim measured the probability density function of the cavity radius using a scanning electron microscope and a differential interference contrast microscope [7]. They assumed that the cavity and cone angle distributions could fit the Poisson and normal distributions, respectively. They showed that the probability density function of the cavity radius for the specimen surface and the probability density function of the cavity cone angle took the following functional forms as expressed by Eqs. (13) and (14), respectively.

$$f(r) = \lambda\exp(-\lambda r) \tag{13}$$

and

$$f(\beta) = \frac{1}{\sqrt{2\pi}s}\exp\{-(\beta - \bar{\beta})^2/(2s^2)\}, \tag{14}$$

where r, λ, β, s, and $\bar{\beta}$ are the radius, the statistical parameter defined in Eq. (13), the half of cone angle, the standard deviation, and the mean half of cone angle, respectively.

To derive the number of cavities which can entrap gas–vapor, Yang and Kim introduced the decisive conditions of gas–vapor entrapment for a cavity proposed by Bankoff and Lorenz [16,17]. They are the cone angle of the cavity and the mouth radius. According to the criteria on the cone angle of the cavity, the cavities with $\beta \geqslant \theta/2$ can not entrap gas or vapor in the cavities and consequently these cavities can not become active nucleation sites. According to the criteria on the mouth radius, the cavities with the mouth size of $R_c \leqslant r \leqslant R_m$, can entrap gas or vapor in the cavities and consequently these cavities can become active nucleation sites. Yang and Kim gave the minimum cavity size, R_c, by Eq. (10). From the geometrical consideration, Yang and Kim derived the maximum cavity size, R_m, as

$$R_m = \sqrt{\frac{4\sigma\cos^2(\theta - \beta)}{\Delta\rho g\{1 - \sin(\theta - \beta)\}[1 + \{\sin(\theta - \beta) - 1\}^2/\{3\cos^2(\theta - \beta)\}]}}. \tag{15}$$

However, it should be noted here that the value of the maximum cavity radius is much greater than technical grade metal cavity radius. For a practical purpose, Yang and Kim introduced the structure upper limit, R_s. The upper limit was determined by allowable error on $\exp(-\lambda R_s)/\exp(-\lambda R_c)$ as

$$R_s = \frac{\ln(\text{Error})}{\lambda} - R_c. \tag{16}$$

Yang and Kim then expressed the real active nucleation site density, N_n, as

$$N_n = \overline{N_n}\int_0^{\theta/2}\frac{1}{\sqrt{2\pi}s}\exp\{-(\beta - \bar{\beta})^2/(2s^2)\}\,d\beta \times \int_{R_c}^{R_s}\lambda\exp(-\lambda r)\,dr, \tag{17}$$

where $\overline{N_n}$ is the average cavity density, which may only depend on the boiling surface material and finish. For a given liquid–surface combination, Yang and Kim approximated Eq. (17) as

$$N_{\mathrm{n}} = \overline{N_{\mathrm{n}}}\phi(\theta)\exp(-\lambda R_{\mathrm{c}}) \approx C\exp(-K/\Delta T_{\mathrm{sat}}), \tag{18}$$

where $\phi(\theta) \equiv \int_0^{\theta/2}\{1/(\sqrt{2\pi}s)\}\exp\{-(\beta-\bar{\beta})^2/(2s^2)\}\,\mathrm{d}\beta$, $C \equiv \overline{N_{\mathrm{n}}}\phi(\theta)$, and $K \equiv (2\lambda\sigma T_{\mathrm{sat}})/(\rho_{\mathrm{g}} i_{\mathrm{fg}})$. The parameter, C, depends on the boiling surface material and finish, and the half of cone angle, but it is a constant for a given liquid–surface combination.

3.3. Wang and Dhir's model (1993)

Wang and Dhir proposed an empirical correlation including the effect of the contact angle on the active nucleation site density during pool boiling of water on a vertical surface based on their experimental data [10]. They performed a pool boiling experiment in saturated water at atmospheric pressure. In the experiment, they utilized mirror-finished copper surfaces prepared by following a well-defined procedure and determined the cumulative number density of the cavities and their shapes with an optical microscope. They changed the wettability of the surface by controlling the degree of oxidation of the surface. The original form of Wang and Dhir's correlation is given by

$$N_{\mathrm{np}} = 5.0\times 10^5(1-\cos\theta)D_{\mathrm{c}}^{-6.0}, \tag{19}$$

where the units of N_{np} and $D_{\mathrm{c}}(=2R_{\mathrm{c}})$ are sites/cm^2 and μm, respectively. In the SI unit, Eq. (19) is represented as

$$N_{\mathrm{np}} = 7.81\times 10^{-29}(1-\cos\theta)R_{\mathrm{c}}^{-6.0}, \tag{20}$$

where the units of N_{np} and R_{c} are sites/m^2 and m, respectively. In Eq. (20), Wang and Dhir gave the critical cavity size by Eq. (10). Wang and Dhir's correlation could reproduce almost all of their data on the active sites on surfaces having contact angles between 90° and 18° within ±60%. Eq. (20) is valid for $D_{\mathrm{c}} < 5.8$ μm, i.e., $R_{\mathrm{c}} < 2.9$ μm, which corresponds to $\Delta T_{\mathrm{W}} > 11.2$ °C for atmospheric water.

3.4. Benjamin and Balakrishnan's model (1997)

Benjamin and Balakrishnan performed an experimental investigation on the nucleation site density during nucleate pool boiling of saturated pure liquids at low-to-moderate heat fluxes [12]. They examined the surface–liquid interaction during the boiling phenomena and its effect on the nucleation site density. They used stainless steel and aluminum with different surface finishes obtained by polishing the surfaces with different grades of emery paper. They utilized the arithmetic average roughness, R_{a}, defined as the average values of the peaks and valleys on the surface to characterize the surface micro-roughness. The liquids used in their study were distilled water, carbon tetrachloride, *n*-hexane, and acetone. They found that the nucleation site density depended on the surface micro-roughness, the surface tension of the liquid, thermo-physical properties of the heating surface and the liquid and the wall superheat. Finally, the following correlation in terms of the wall superheat, ΔT_{w}, the Prandtl number, Pr, a surface–liquid interaction parameter, γ, and a dimensionless surface roughness parameter, Θ, was proposed.

$$N_{\mathrm{np}} = 218.8Pr^{1.63}\left(\frac{1}{\gamma}\right)\Theta^{-0.4}\Delta T_{\mathrm{w}}^3, \tag{21}$$

Prandlt number, Pr, is defined as

$$Pr \equiv \frac{C_{pf}\mu_{\mathrm{f}}}{\kappa_{\mathrm{f}}} \tag{22}$$

and accounts for the physical properties of the liquid being boiled. C_{pf}, μ_{f}, and κ_{f} are the liquid specific heat at constant pressure, the liquid viscosity, and the liquid thermal conductivity, respectively. The surface–liquid interaction parameter, γ, is defined by

$$\gamma \equiv \left(\frac{\kappa_{\mathrm{w}}\rho_{\mathrm{w}}C_{pw}}{\kappa_{\mathrm{f}}\rho_{\mathrm{f}}C_{pf}}\right)^{1/2}, \tag{23}$$

where C_{pw}, ρ_{w}, and κ_{w} are the wall specific heat at constant pressure, the wall density, and the wall thermal conductivity, respectively. The dimensionless surface roughness parameter, Θ, is given by

$$\Theta = 14.5 - 4.5\left(\frac{R_{\mathrm{a}}P}{\sigma}\right) + \left(\frac{R_{\mathrm{a}}P}{\sigma}\right)^{0.4}. \tag{24}$$

The range of parameters covered in developing and validating the correlation were $1.7 < Pr < 5$, $4.7 < \gamma < 93$, $0.02\ \mathrm{mm} < R_{\mathrm{a}} < 1.17\ \mathrm{mm}$, $5\ \mathrm{K} < \Delta T_{\mathrm{w}} < 25\ \mathrm{K}$; $13\times 10^{-3}\ \mathrm{N/m} < \sigma < 59\times 10^{-3}\ \mathrm{N/m}$, $2.2 < \Theta < 14$.

3.5. Basu, Warrier and Dhir's model (2002)

Basu et al. proposed an empirical correlation including the effect of the contact angle on the active nucleation site density during forced convective boiling of water on a vertical surface based on their experimental data [15]. They performed subcooled boiling experiment at atmospheric pressure. In the experiments, they utilized mirror-finished copper surfaces prepared by following a well-defined procedure. They changed the wettability of the surface by controlling the degree of oxidation of the surface. The original form of Basu et al. correlation is given by

$$\begin{aligned} N_{\mathrm{nc}} &= 0.34(1-\cos\theta)\Delta T_{\mathrm{w}}^{2.0} \quad \Delta T_{\mathrm{ONB}} < \Delta T_{\mathrm{w}} < 15\ \mathrm{K}, \\ N_{\mathrm{nc}} &= 3.4\times 10^{-5}(1-\cos\theta)\Delta T_{\mathrm{w}}^{5.3} \quad 15\ \mathrm{K} \leqslant \Delta T_{\mathrm{w}}, \end{aligned} \tag{25}$$

where the units of N_{nc} and ΔT_{w} are sites/cm^2 and K, respectively. ΔT_{ONB} is the wall superheat at the onset of the nucleate boiling. In the SI unit, Eq. (25) is represented as

$$N_{nc} = 0.34 \times 10^4 (1 - \cos\theta)\Delta T_w^{2.0} \quad \Delta T_{ONB} < \Delta T_w < 15 \text{ K},$$

$$N_{nc} = 3.4 \times 10^{-1} (1 - \cos\theta)\Delta T_w^{5.3} \quad 15 \text{ K} \leqslant \Delta T_w, \qquad (26)$$

where the unit of N_{nc} is sites/m^2. Basu et al.'s correlation could reproduce almost all of their data on the active sites on surfaces having contact angles between 90° and 30° within ±40%. The range of parameters covered for the flat plate test surface were 124 kg/m^2 s $< G <$ 886 kg/m^2 s, 6.6 K $< \Delta T_{sub,in} <$ 52.5 K, 2.5 W/cm^2 $< q_w <$ 96 W/cm^2, 30° $< \theta <$ 90°.

4. Modeling of active nucleation site density

It is found that there is a difference in the exponent to the wall superheat among the existing correlations explained in the previous section. Kocamustafaogullari and Ishii's correlation indicated the exponent to be 4.4 [6], whereas Benjamin and Balakrishnan claimed the exponent to be 3 [12]. Basu et al. showed that the exponent is 2.0 or 5.3 depending on the wall superheat [15]. Thus, it is anticipated that the exponent may vary with the critical cavity size, which is a function of the wall superheat. To prove this hypothesis, a theoretical analysis on the active nucleation site density will be performed based on Yang and Kim's approach [7].

Yang and Kim assumed that the cavity distribution could fit the Poisson distribution. By applying the χ^2-test on the measurements, the probability density function of the cavity radius for the specimen surface was given by Eq. (13). Thus, the number of cavity, $n_c^r(r)$, in a certain range of the cavity radius, Δr, and measuring area, A, is given by

$$n_c^r(r) = \overline{N_n} A f(r)\Delta r = \overline{N_n} A \lambda \exp(-\lambda r)\Delta r. \qquad (27)$$

The distribution of the cavity number is plotted in terms of the radius of the cavity in Fig. 1. The solid line indicates the cavity number distribution calculated by Eq. (27) with $\lambda = 0.980$ μm^{-1} and $\overline{N_n} A \lambda \Delta r = 14.5$ sites. Eq. (27) seems to reproduce the cavity number distribution against the cavity radius fairly well in the tested surface. In the measuring area, the number of the cavity, $n_c^r(r)$, takes a value of 14.5 sites at $r = 0$ μm. However, physically, this might not be sound. In reality, the number of the cavity should go to infinity for $r \to 0$ μm.

On the other hand, Yang and Kim assumed that the angle distribution could fit the normal distributions. By applying the χ^2-test on the measurements, the probability density function of the cavity cone angle for the specimen surface was given by Eq. (14). Thus, the number of cavity, $n_c^\beta(r)$, in a certain range of the half of cone angle, $\Delta\beta$, and measuring area, A, is given by

$$n_c^\beta(\beta) = \overline{N_n} A f(\beta)\Delta\beta = \frac{\overline{N_n} A}{\sqrt{2\pi}s} \exp\{-(\beta - \bar{\beta})^2/(2s^2)\}\Delta\beta. \qquad (28)$$

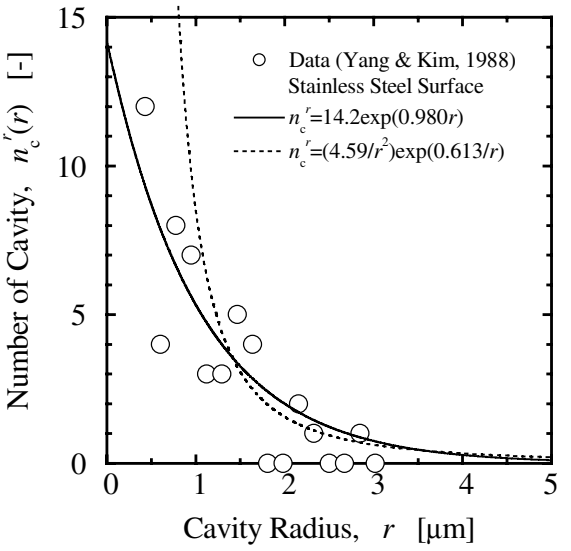

Fig. 1. Cavity number distribution in terms of cavity radius.

The distribution of the cavity number is plotted in terms of the half of the cone angle of the cavity in Fig. 2. The solid line indicates the cavity number distribution calculated by Eq. (28) with $s = 0.285$ rad, $\bar{\beta} = 0.374$ rad, and $\overline{N_n} A \Delta\beta/\sqrt{2\pi}s = 12.2$ sites. Eq. (28) seems to reproduce the cavity number distribution against the half of the cone angle fairly well in the tested surface. In the measuring area, the number of the cavity, $n_c^\beta(r)$, takes a value of 5.13 at $\beta = 0$ rad. However, physically, this might not be sound. In reality, the number of the cavity should go to zero for $\beta \to 0$ rad.

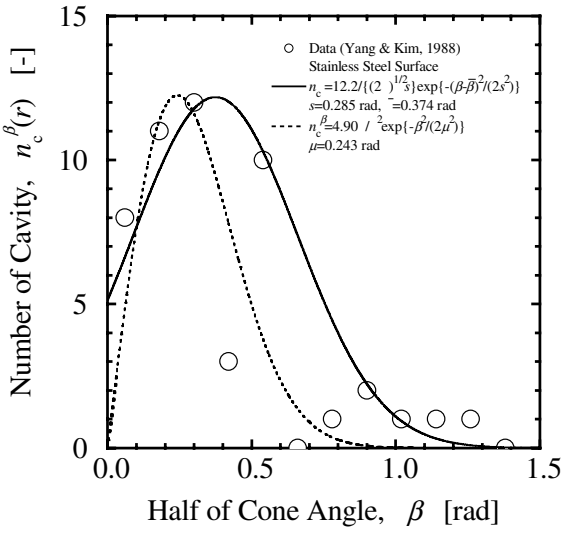

Fig. 2. Cavity number distribution in terms of half of cavity cone angle.

Yang and Kim expressed the active nucleation site density by Eq. (18) for a given liquid–surface combination. The value of K is 31.9 K for saturated water at atmospheric pressure. The dependence of the active nucleation site density on the gas superheat estimated by Yang and Kim's function is shown in Fig. 3. In this figure, non-dimensional active nucleation site density, $N^*_{n,Y-K}$ is defined as

$$N^*_{n,Y-K} = N_n/C \approx \exp(-K/\Delta T_{sat}). \quad (29)$$

The broken line in Fig. 3 indicates the prediction by Eq. (29) with $K = 31.9$ K. For $\Delta T_{sat} > 10$ K, the obtained slope of the active nucleation site density against the gas superheat is much gentler than that reported by various investigators. Griffith and Wallis [18] reported that a plot of the active nucleation site density against the gas superheat was almost vertical, since a very small increase in temperature would be sufficient to activate another cavity. However, Yang and Kim's functional form indicates that the active nucleation site density asymptotically approaches a certain value with increasing the gas superheat. Kocamustafaogullari and Ishii's correlation can be recast with the approximation indicated by Eq. (10) as

$$N_n \propto \Delta T_{sat}^{4.4}. \quad (30)$$

The slope predicted by Eq. (29) is much gentler than 4.4 suggested by Kocamustafaogullari and Ishii's correlation. For 4 K $\leqslant \Delta T_{sat} \leqslant$ 10 K, the slope predicted by Eq. (29) approximately agrees with the slope suggested by Kocamustafaogullari and Ishii's correlation. On the other hand, for $\Delta T_{sat} < 4$ K, the obtained slope of the active nucleation site density against the gas superheat is much steeper than that reported by various investigators. Recently, Basu et al. showed experimentally that for $\Delta T_{ONB} \leqslant \Delta T_{sat} \leqslant 15$ K the slope was 2.0 for mirror-finished stainless steel surface at atmospheric pressure [15]. In Fig. 3, the sensitivity analysis to obtain the effect of the parameter K on the $N^*_{n,Y-K} - \Delta T_{sat}$ relationship is performed by changing the K-parameter. The similar results explained above are obtained for changed K-parameter such as $K = 10.0$ and 100 K.

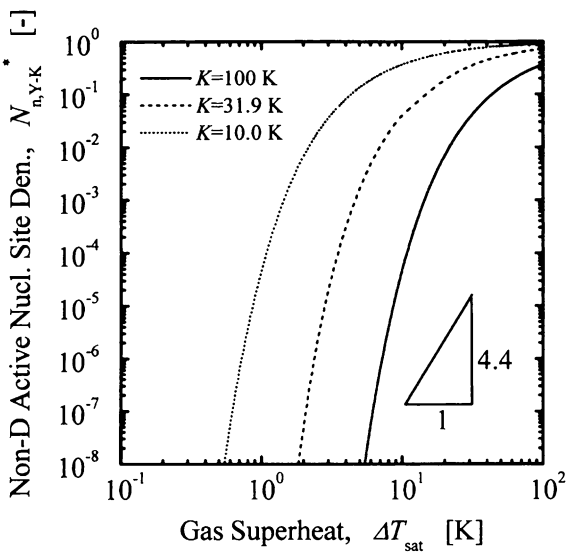

Fig. 3. Dependence of non-dimensional active nucleation site density on gas superheat.

Based on the above detailed discussions, although the basic concept of Yang and Kim's model might be sound, the approximated functions of the number of the cavity in terms of the cavity radius and the half of the cone angle might not be appropriate. In view of this, physically sound functions are introduced here to complete the Yang and Kim's approach. One of the promising functions to approximate the cavity number distribution function of the cavity radius is expressed as

$$f'(r) = \frac{\lambda'}{r^2}\exp\left(\frac{\lambda'}{r}\right), \quad (31)$$

where λ' is a characteristic length scale. Thus, the number of cavity, $n^r_c(r)$, in a certain range of the cavity radius, Δr, and measuring area, A, is given by

$$n^r_c(r) = \overline{N_n} A f'(r)\Delta r = \frac{\overline{N_n} A \lambda'}{r^2}\exp\left(\frac{\lambda'}{r}\right)\Delta r. \quad (32)$$

The broken line in Fig. 1 indicates the cavity number distribution calculated by Eq. (32) with $\lambda' = 0.613$ μm and $\overline{N_n} A \lambda' \Delta r = 4.59$ sites m^2. Eq. (32) seems to reproduce the cavity number distribution against the cavity radius fairly well in the tested surface. The number of the cavity, $n^r_c(r)$, approaches infinity as $r \to 0$ μm, which is physically sound.

On the other hand, one of the promising functions to approximate the cavity number distribution function of the half of the cavity cone angle is expressed by the Rayleigh distribution as

$$f'(\beta) = \frac{\beta}{\mu^2}\exp\{-\beta^2/(2\mu^2)\}, \quad (33)$$

where μ is a characteristic cone angle scale. Thus, the number of cavity, $n^\beta_c(r)$, in a certain range of the half of cone angle, $\Delta\beta$, and measuring area, A, is given by

$$n^\beta_c(\beta) = \overline{N_n} A f'(\beta)\Delta\beta = \frac{\overline{N_n} A \beta}{\mu^2}\exp\{-\beta^2/(2\mu^2)\}\Delta\beta. \quad (34)$$

The broken line in Fig. 2 indicate the cavity number distribution calculated by Eq. (34) with $\mu = 0.243$ rad and $\overline{N_n} A \Delta\beta = 4.90$ sites. Eq. (34) seems to reproduce the cavity number distribution against the half of the cone angle fairly well in the tested surface. The number of the

cavity approaches zero as $\beta \to 0$ rad, which is physically sound.

From Eqs. (31) and (33), the active nucleation site density can be represented by

$$\begin{aligned} N_n &= \overline{N_n} \int_0^{\theta/2} f'(\beta)\,d\beta \int_{R_c}^{R_{max}} f'(r)\,dr \\ &= \overline{N_n} \int_0^{\theta/2} \frac{\beta}{\mu^2} \exp\{-\beta^2/(2\mu^2)\}\,d\beta \int_{R_c}^{R_{max}} \frac{\lambda'}{r^2} \\ &\quad \times \exp\left(\frac{\lambda'}{r}\right) dr \\ &= \overline{N_n}\left\{1 - \exp\left(-\frac{\theta^2}{8\mu^2}\right)\right\}\left\{\exp\left(\frac{\lambda'}{R_c}\right) \right. \\ &\quad \left. - \exp\left(\frac{\lambda'}{R_{max}}\right)\right\} \\ &= \overline{N_n}\phi'(\theta)\phi'(r), \end{aligned} \tag{35}$$

where

$$\phi'(\theta) = \int_0^{\theta/2} f'(\beta)\,d\beta = 1 - \exp\left(-\frac{\theta^2}{8\mu^2}\right), \tag{36}$$

$$\begin{aligned} \phi'(r) &= \int_{R_c}^{R_{max}} f'(r)\,dr \\ &= \exp\left(\frac{\lambda'}{R_c}\right) - \exp\left(\frac{\lambda'}{R_{max}}\right) \end{aligned} \tag{37}$$

and R_{max} is the maximum cavity size. This expression is general if we use the maximum cavity size. However, this will lead to a highly complicated correlation for the active nucleation site density. Therefore, it is desirable to obtain a simple expression, which satisfies the overall physical phenomenon.

First, consider the case of $\Delta T_{sat} = 0$ K, namely $R_c = \infty$ m, resulting in $\exp(\lambda'/R_c) = 1$. Under this condition, N_n should be 0 sites/m^2, which means that $\exp(\lambda'/R_{max})$ should be 1. Therefore, Eq. (35) reduces to

$$\begin{aligned} N_n &= \overline{N_n}\left\{1 - \exp\left(-\frac{\theta^2}{8\mu^2}\right)\right\}\left\{\exp\left(\frac{\lambda'}{R_c}\right) - 1\right\} \\ &\approx \overline{N_n}\left\{1 - \exp\left(-\frac{\theta^2}{8\mu^2}\right)\right\}\{\exp(K_1\Delta T_{sat}) - 1\}, \end{aligned} \tag{38}$$

where $K_1 = (\lambda'\rho_g i_{fg})/(2\sigma T_{sat})$. The above approximation holds for $\rho_g \ll \rho_f$ and $i_{fg}(T_g - T_{sat})/(RT_gT_{sat}) \ll 1$.

Second, consider the case of extremely large ΔT_{sat} namely $R_c \approx 0$ m, resulting in $\exp(\lambda/R_c) = \infty$. Thus, for extremely large ΔT_{sat}, the active nucleation site density becomes infinity, which may be sound physically. Therefore, it may be concluded from these two limiting conditions that the general expression for N_n can be given approximately by Eq. (38).

In what follows, the active nucleation site density on the cavity size and the contact angle will be discussed based on Eq. (38). First, to examine the dependence of the active nucleation site density on the cavity size the predictions by Eq. (38) for a given liquid–surface combination, namely constant contact angle, are plotted in Fig. 4. In this figure, Eq. (38) is non-dimensionalized as follows:

$$\begin{aligned} N^*_{n,H\text{–}I} &= \frac{N_n}{\overline{N_n}[1 - \exp\{-\theta^2/(8\mu^2)\}]} \\ &= \exp\left(\frac{\lambda'}{R_c}\right) - 1 \approx \exp(K_1\Delta T_{sat}) - 1. \end{aligned} \tag{39}$$

For lower ΔT_{sat}, the active nucleation site density gradually increases with the gas superheat, whereas for higher ΔT_{sat}, the active nucleation site density steeply increases with the gas superheat. Thus, the slope is changing with increasing the gas superheat. Such tendency agrees with the observations by various investigators [6,9,10,12,15].

It is interesting to note here that in a certain range of ΔT_{sat} Eq. (38) can be approximated by

$$N_n = C_1 R_c^{-m}, \tag{40}$$

where C_1 and m are a constant for a given liquid–surface combination and flow condition and an exponent, respectively. Eq. (40) has the same functional form as Kocamustafaogullari and Ishii's correlation.

Next, the dependence of the active nucleation site density on the contact angle will be discussed based on Eq. (38). Eq. (38) suggests that the active nucleation site

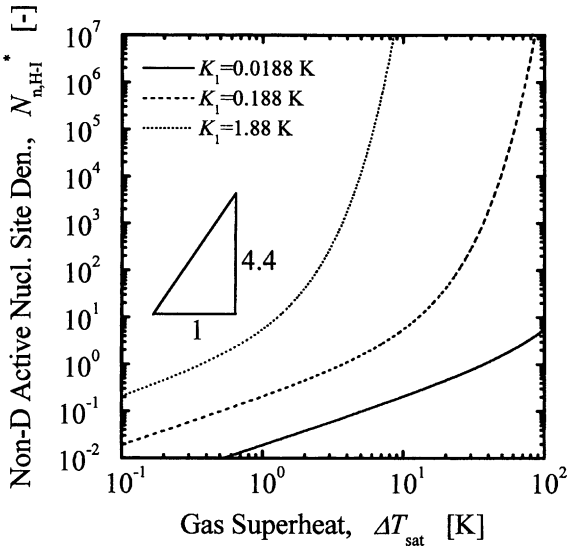

Fig. 4. Dependence of non-dimensional active nucleation site density on gas superheat.

density is a function of the contact angle. Kocamustafaogullari and Ishii's correlation can be recast as follows:

$$N_{\mathrm{n}} = 9.21 \times 10^{-20} \rho^{*-0.96} (1 + 0.0049\rho^{*})^{4.13} \times \theta^{2.4} \left(\frac{\sigma}{g\Delta\rho} \right)^{1.2} R_{\mathrm{c}}^{-4.4}. \quad (41)$$

Thus, Kocamustafaogullari and Ishii's correlation shows the dependence of the active nucleation site density on the contact angle to be presented by $\theta^{2.4}$. Basu et al. also represented the dependence of the active nucleation site density on the contact angle as a function of $1 - \cos\theta$. Fig. 5 compares Eq. (36) with the dependences of the active nucleation site density on the contact angle proposed by Kocamustafaogullari and Ishii, and Basu et al. It should be noted here that the coefficients for $\theta^{2.4}$ and $1 - \cos\theta$, and the parameter, μ, in Eq. (36) are determined so as that three functions give closest values one another. The functional dependence represented by $\theta^{2.4}$ can be approximated by Eq. (36) satisfactorily for $\theta \leqslant 90°$. The functional dependence represented by $1 - \cos\theta$ can also be approximated by Eq. (36) very well. This result indicates that the functional form obtained by the parametric study, $\theta^{2.4}$, and the functional form determined empirically, $1 - \cos\theta$, can approximately represent the true functional dependence of the active nucleation site density on the contact angle. Thus, it is concluded that Eq. (38) would be promising to develop a general correlation to predict the active nucleation site density. In what follows, the derived equation, Eq. (38), will be evaluated by existing data.

5. Evaluation of active nucleation site density model

First, the derived equation, Eq. (38) will be evaluated by using Basu et al.'s data [15], which were taken in subcooled water boiling flows at atmospheric pressure with well-prepared metal surface as parameters of mass velocity, inlet subcooling and contact angle. Fig. 6 shows the comparison of Eq. (38) with the data. In Fig. 6, the solid, broken, and dotted lines indicate the predictions by Eq. (38), Kocamustafaogullari and Ishii's equation presented by Eq. (41), and Basu et al.'s correlation presented by Eq. (26), respectively. Here, the parameters in Eq. (38) are determined by Basu et al.'s data to be $\overline{N_{\mathrm{n}}} = 4.72 \times 10^5$ sites/m^2 and $\lambda' = 2.50 \times 10^{-6}$ m. It should be noted here that the gas superheat in Eq. (38) is approximated to be the wall superheat. Basu et al. proved experimentally no systematic effect of mass velocity and liquid subcooling on the active nucleation site density for a given liquid–surface combination [15]. In other words, for a given contact angle, the dependence of the active nucleation site density on the wall superheat is independent of both mass velocity and the subcooling, and the nucleation site density depends only on static contact angle and wall superheat. Their observation indicates that the gas superheat, ΔT_{sat} can be approximated to be the wall superheat, ΔT_{w}.

It can be seen from Fig. 6 that Eq. (38) can represent a proper trend of the data satisfactorily. Thus, Eq. (38) would be a promising functional form to develop a general correlation of the active nucleation site density. Here, it is assumed that the active nucleation site density is also influenced by both the surface conditions and the thermo-physical properties of the fluid. For a given

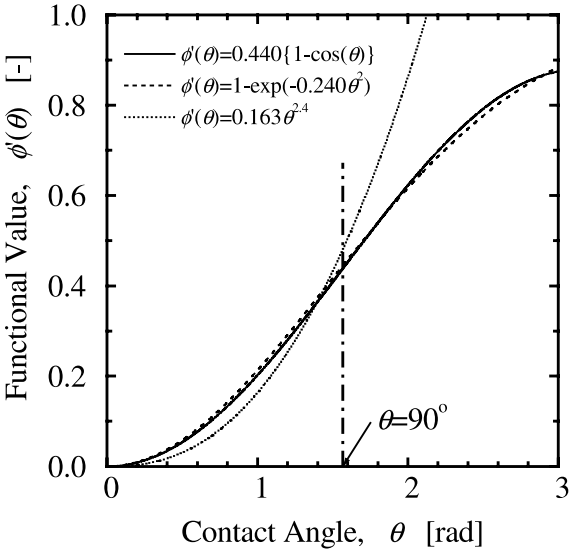

Fig. 5. Dependence of integrated PDF function, $\phi'(\theta)$, on contact angle.

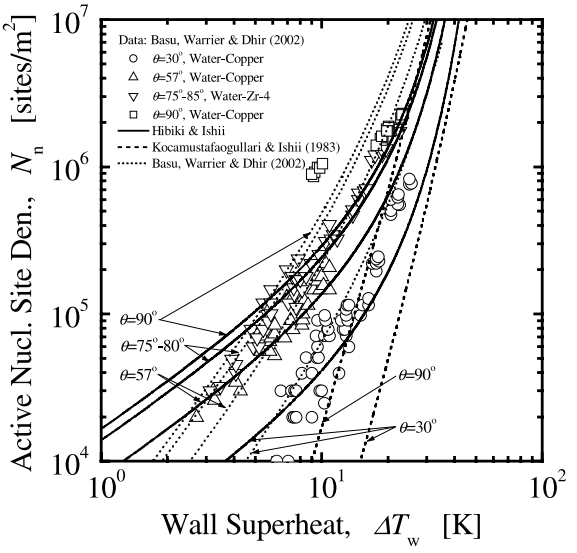

Fig. 6. Comparison of newly developed active nucleation site density model with Basu et al.'s data.

fluid, properties may be described as a function of pressure only, and realizing the significance of the minimum cavity size as an important surface parameter, the following equation is proposed to generalize Eq. (38) as

$$N_n^+ \equiv \frac{N_n}{\overline{N_n}[1-\exp\{-\theta^2/(8\mu^2)\}]} = \exp\{f(\rho^+)/R_c^+\} - 1$$

or

$$\ln\left[\frac{N_n}{\overline{N_n}[1-\exp\{-\theta^2/(8\mu^2)\}]} + 1\right] = f(\rho^+)/R_c^+, \qquad (42)$$

where $f(\rho^+)$ is a function of the logarithmic non-dimensional density difference, ρ^+ defined by $\log(\Delta\rho/\rho_g)$ and R_c^+ is the non-dimensional critical cavity radius defined by R_c/λ'. Finally, fitting the water data [19] with Eq. (42), the function, $f(\rho^+)$, was determined and the final result can be represented by

$$f(\rho^+) = -0.01064 + 0.48246\rho^+ - 0.22712\rho^{+2} + 0.05468\rho^{+3}. \qquad (43)$$

It should be noted here that Eq. (9) giving R_c might not be valid strictly at high pressure since it has been derived under two assumptions that the expansion ratio, ρ_g/ρ_f, is small and the equation of state of ideal gas holds. Thus, Eq. (43) can be considered to include the total effect of the estimation error of R_c due to these invalid assumptions at high pressure on the active nucleation site density.

Fig. 7 compares Eq. (42) with Eq. (43) with the water data [19]. The solid lines indicate the predictions by Eq. (42) with Eq. (43). It should be noted here that the data in Fig. 7 were cited from Kocamustafaogullari and Ishii's paper [6]. They calculated the active nucleation site data from experimental values of the heat transfer coefficient and the gas superheat with their heat transfer correlation [6]. Thus, the high pressure data rather scatter. However, the newly developed model gives fairly good predictions of the active nucleation site density.

Here, to discuss further implicit physical meaning of $f(\rho^+)$, Eq. (42) is further recast for $\exp\{f(\rho^+)/R_c^+\} \gg 1$ as

$$\begin{aligned} N_n^+ &\equiv \frac{N_n}{\overline{N_n'}[1-\exp\{-\theta^2/(8\mu^2)\}]} = \exp\{f(\rho^+)/R_c^+\} - 1 \\ &= \exp[\{f(\rho^+)-1\}/R_c^+]\exp(1/R_c^+) - 1 \\ &\approx \exp[\{f(\rho^+)-1\}/R_c^+]\exp(1/R_c^+) \end{aligned}$$

or

$$N_n \approx \overline{N_n}\exp[\{f(\rho^+)-1\}/R_c^+]\left\{1-\exp\left(-\frac{\theta^2}{8\mu^2}\right)\right\} \times \exp(1/R_c^+). \qquad (44)$$

In the comparisons shown in Fig. 7, the value of the contact angle at room temperature was used. The contact angle may be a weak function of the temperature at relatively low temperature, whereas it may be a strong function of the temperature at relatively high temperature. For example, Bernardin et al. [20] reported the contact angle temperature dependence for water droplets on practical aluminum surfaces. For $T_w \leqslant 130$ °C ($=403$ K), the value of the contact angle is almost the same as that at the room temperature, whereas for $T_w > 130$ °C, the value gradually decreases with increasing the surface temperature and finally reach to zero at the critical temperature, namely $T_w = 374.15$ °C ($=647.3$ K). The term of $\exp[\{f(\rho^+)-1\}/R_c^+]$ in Eq. (44) is a function of the thermo-physical properties as well as T_w and T_{sat}. Therefore, the term of $\exp[\{f(\rho^+)-1\}/R_c^+]$ might implicitly represent the effect of the temperature on the contact angle. Fig. 8 shows the dependence of $f(\rho^+)$ on ρ^+. The correction factor at $\rho^+ = 3$ and 0 roughly corresponds to $T_w = 100$ °C ($=373.15$ K) and $T_w = 374.15$ °C ($=647.3$ K) for water, respectively. The correction factor gradually decreases with decreasing ρ^+, namely increasing T_w, and finally

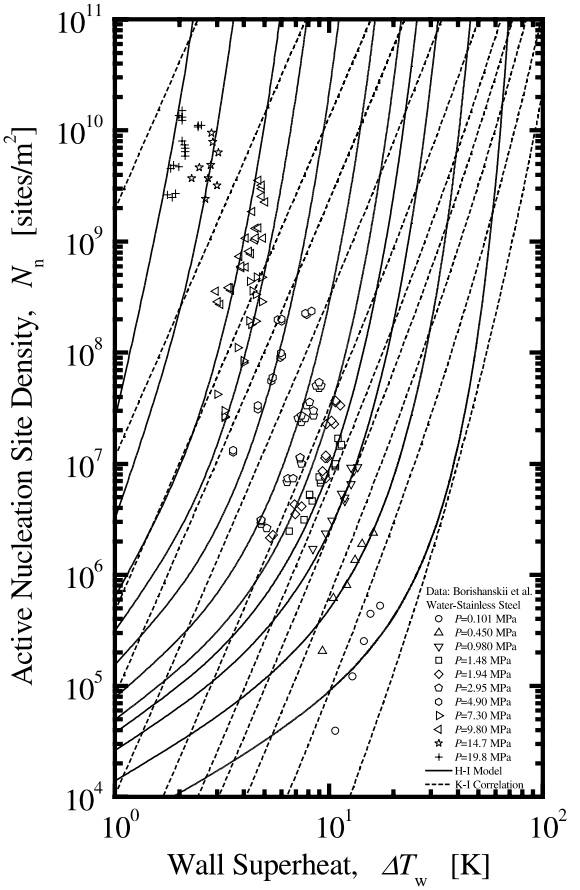

Fig. 7. Comparison of newly developed active nucleation site density model with high-pressure water data.

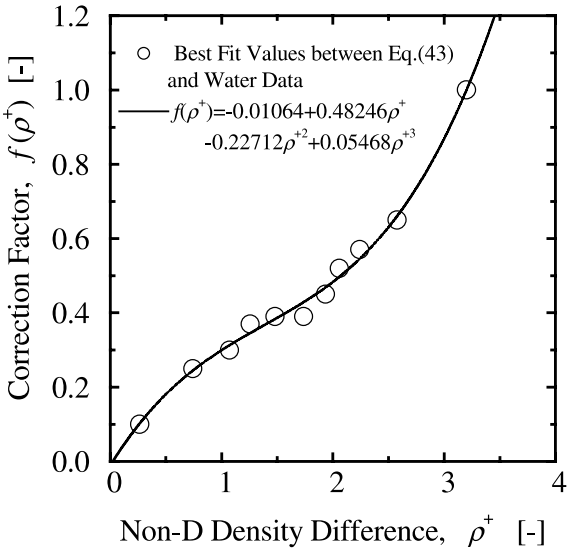

Fig. 8. Dependence of correction factor on the density difference.

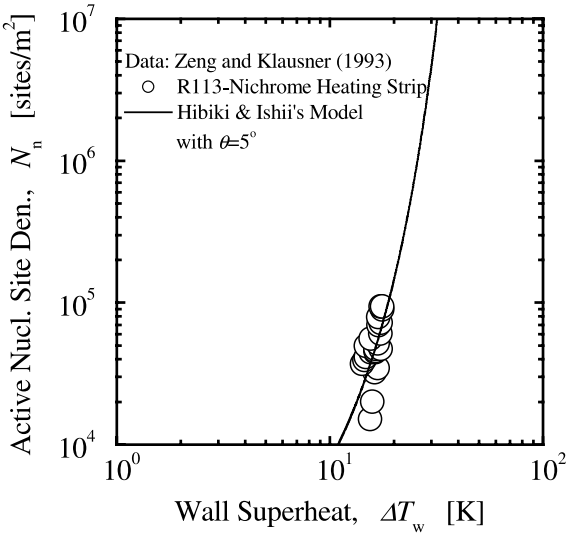

Fig. 9. Comparison of newly developed active nucleation site density model with Zeng and Klausner's data.

become zero at the critical point, namely $\rho^+ = 0$ or $T_w = 374.15$ °C. Interestingly, this tendency agrees with the dependence of the contact angle on the temperature [20].

Fig. 7 also shows the comparison between the newly developed model and Kocamustafaogullari and Ishii's correlation indicated by the broken lines. The newly developed model agrees with Kocamustafaogullari and Ishii's correlation for a relatively small critical cavity size, namely a relatively high wall superheat. Thus, Kocamustafaogullari and Ishii's correlation is considered to be the approximated form of the newly developed model in this study, Eq. (42) with Eq. (43). This means that Eq. (42) with Eq. (43) will give fairly good predictions for the extensive data which were used for evaluating Kocamustafaogullari and Ishii's correlation. The newly developed model of the active nucleation site density, Eq. (42) with Eq. (43) can also be reduced to Basu et al.'s correlation in a certain flow condition (see Fig. 6).

Further comparisons between the newly developed model and some existing data are presented in Figs. 9 and 10. Fig. 9 compares the newly developed model with the data obtained by Zeng and Klausner in a forced convective R-113 in a 25×25 mm test section with a nichrome heating strip [9]. The contact angle was not given in the paper. Judging from the similarity of physical properties between the other Freons and R-113 and the contact angle of the other Freons [15], the contact angle may be around 5°. Thus, the solid line in Fig. 9 indicates the prediction by the model, Eq. (42), with $\theta = 5°$. Good agreement is obtained between the newly developed model, Eq. (42), and the data. Fig. 10 compares the newly

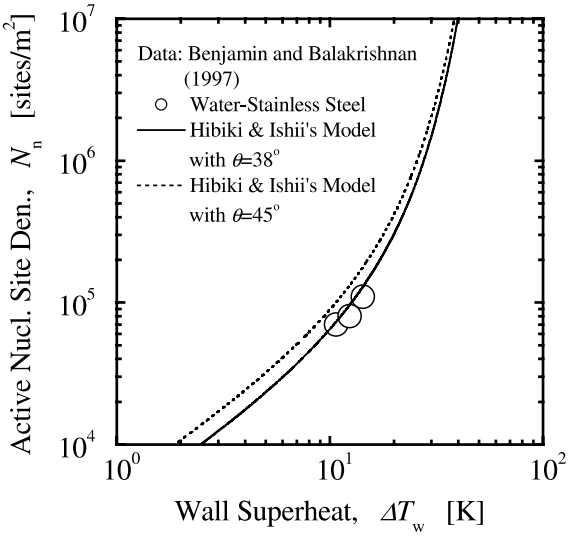

Fig. 10. Comparison of newly developed active nucleation site density model with Benjamin and Balakrishnan's data.

developed model with the data obtained by Benjamin and Balakrishnan in a pool boiling [12]. Since they correlated the active nucleation site density with surface condition such as surface roughness, the contact angle for water-stainless steel was not given in the paper. Recently, Kandlikar and Steinke [21] measured the dependence of the contact angle on the surface roughness. Judging from the surface roughness given by Benjamin and Balakrishnan and the dependence of the contact angle on the surface roughness measured by Kandlikar

and Steinke, the contact angle for the water-stainless steel in the Benjamin and Balakrishnan's data may be around 30°-to-40°. Here, the contact angle (= 38°) reported by Bergles and Rohsenow [22] is used in the prediction, see the solid line. To show the effect of the contact angle on the active nucleation site density, the prediction with $\theta = 45°$ is also indicated by the dotted line in Fig. 10. Good agreement is obtained between the newly developed model, Eq. (42), and the data. Fig. 11 shows the comparison of the newly developed active nucleation site density model with the existing data. Reasonably good agreement is obtained between the newly developed model and the data. The average prediction error for the active nucleation site density measured directly [9,12,15] is estimated to be ±28.5%. The average prediction error for all the active nucleation site density data including the scattering high-pressure data calculated indirectly by the heat transfer data [19] is estimated to be ±62.4%. Thus, the newly developed model gives fairly good predictions over rather wide range of the flow conditions (0 kg/m^2 s $\leqslant G \leqslant$ 886 kg/m^2 s; 0.101 MPa $\leqslant P \leqslant$ 19.8 MPa; 5° $\leqslant \theta \leqslant$ 90°; 1.00×10^4 sites/m^2 $\leqslant N_n \leqslant 1.51 \times 10^{10}$ sites/m^2).

To summarize the present study, the newly developed model for the active nucleation site density is given below.

$$N_n = \overline{N_n}\left\{1 - \exp\left(-\frac{\theta^2}{8\mu^2}\right)\right\}\left[\exp\left\{f(\rho^+)\frac{\lambda'}{R_c}\right\} - 1\right], \tag{45}$$

where $\overline{N_n} = 4.72 \times 10^5$ sites/m^2, $\mu = 0.722$ rad, $\lambda' = 2.50 \times 10^{-6}$ m,

$$R_c = \frac{2\sigma\{1 + (\rho_g/\rho_f)\}/P_f}{\exp\{i_{fg}(T_g - T_{sat})/(RT_gT_{sat})\} - 1},$$

$$f(\rho^+) = -0.01064 + 0.48246\rho^+ - 0.22712\rho^{+^2} + 0.05468\rho^{+^3},$$

$$\rho^+ = \log(\rho^*)$$

and $\rho^* = \Delta\rho/\rho_g$. Here, R is the gas constant based on a molecular weight. For example, the value of R for water vapor is 462 J/(kg K) (= 8.31 J/(mol K)/(18.0×10^{-3} kg/mol)).

To further generalize the newly developed model of the active nucleation site density, it should be evaluated by many rigorous experimental data of the active nucleation site density by well-designed experiment to be performed in a future study. The function, $f(\rho^+)$, which implicitly includes the contact angle dependence on the temperature may be replaced by rigorous measurement of the contact angle dependence on the temperature to be performed in a future study. The recent study of Kandlikar and Steinke [21] may imply a strong correlation between the contact angle and the surface roughness. The dependence of the active nucleation site density on the surface roughness may be explained in terms of the contact angle in a future study.

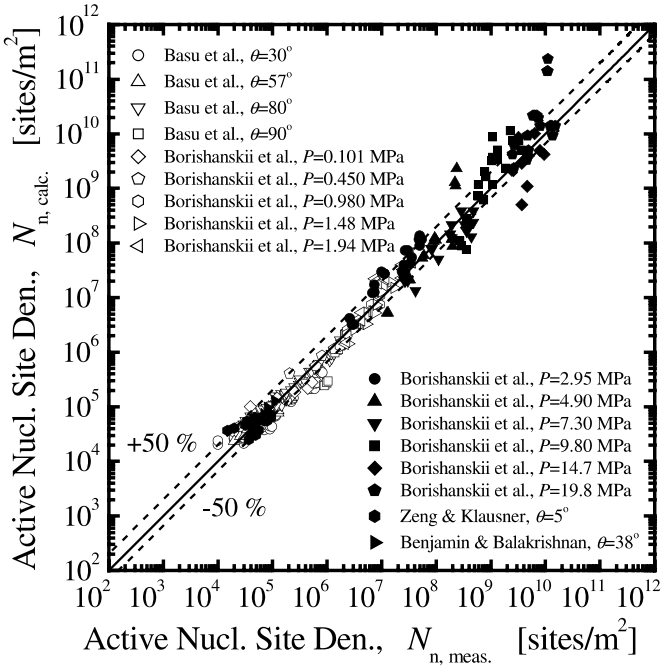

Fig. 11. Comparison of newly developed active nucleation site density model with existing data.

6. Conclusions

Realizing the significance of the active nucleation site density as an important parameter for predicting the interfacial area concentration in a two-fluid model formulation, the active nucleation site density has been modeled and evaluated by existing experimental data taken in pool boiling and forced convective boiling systems. The important results obtained are summarized as follows:

(1) One-dimensional interfacial area transport equation for boiling flow system has been formulated by taking into account the homogeneous and heterogeneous bulk liquid nucleation, the wall cavity nucleation, the bubble collapse, the bubble breakup and coalescence, and the bubble expansion or shrinkage. The significance of these sink and source terms in the heated boiling channel was discussed.
(2) Extensive literature survey has been conducted for recent correlations developed for predicting the active nucleation site density. In general, it has been found that the active nucleation site density is a function of the wall superheat. However, it has been pointed out that there is a difference in the exponent to the wall superheat among the existing correlations.
(3) The active nucleation site density has been modeled mechanistically by knowledge of the size and cone angle distributions of cavities that are actually present on the surface. The newly developed model has been validated by various active nucleation site density data taken in pool boiling and convective flow boiling systems. The newly developed model clearly shows that the active nucleation site density is a function of the critical cavity size and the contact angle, and the model can explain the dependence of the active nucleation site density on the wall superheat reported by various investigators. The newly developed model can give fairly good predictions over rather wide range of the flow conditions ($0\ \text{kg/m}^2\,\text{s} \leqslant G \leqslant 886\ \text{kg/m}^2\,\text{s}$; $0.101\ \text{MPa} \leqslant P \leqslant 19.8\ \text{MPa}$; $5^\circ \leqslant \theta \leqslant 90^\circ$; $1.00 \times 10^4\ \text{sites/m}^2 \leqslant N_n \leqslant 1.51 \times 10^{10}\ \text{sites/m}^2$). The average prediction error for the active nucleation site density measured directly is estimated to be $\pm 28.5\%$. The average prediction error for all the active nucleation site density data including the scattering high-pressure data calculated indirectly by the heat transfer data is estimated to be $\pm 62.4\%$.

Acknowledgements

The authors would like to express their special thanks to Professor Jean-Marc Delhaye (Clemson University, USA) and Mr. Rong Situ (Purdue University, USA) for their fruitful discussions. The research project was supported by the Tokyo Electric Power Company (TEPCO). The authors would like to express their sincere appreciation for the support and guidance from Dr. Mori of the TEPCO. Part of this work was supported by grant-in-aid for scientific research from the Ministry of Education, Science, Sport and Culture (no. 14580542).

References

[1] T. Hibiki, M. Ishii, One-group interfacial area transport of bubbly flows in vertical round tubes, Int. J. Heat Mass Transfer 43 (2000) 2711–2726.
[2] G. Kocamustafaogullari, M. Ishii, Foundation of the interfacial area transport equation and its closure relations, Int. J. Heat Mass Transfer 38 (1995) 481–493.
[3] T. Hibiki, M. Ishii, Development of one-group interfacial area transport equation in bubbly flow systems, Int. J. Heat Mass Transfer 45 (2002) 2351–2372.
[4] T. Hibiki, M. Ishii, Two-group interfacial area transport equations at bubbly-to-slug flow transition, Nucl. Eng. Design 202 (2000) 39–76.
[5] M.D. Bartel, M. Ishii, T. Masukawa, Y. Mi, R. Situ, Interfacial area measurements in subcooled flow boiling, Nucl. Eng. Design 210 (2001) 135–155.
[6] G. Kocamustafaogullari, M. Ishii, Interfacial area and nucleation site density in boiling systems, Int. J. Heat Mass Transfer 26 (1983) 1377–1387.
[7] S.R. Yang, R.H. Kim, A mathematical-model of the pool boiling nucleation site density in terms of the surface characteristics, Int. J. Heat Mass Transfer 31 (1988) 1127–1135.
[8] G. Barthau, Active nucleation site density and pool boiling heat transfer—an experimental study, Int. J. Heat Mass Transfer 35 (1992) 271–278.
[9] L.Z. Zeng, J.F. Klausner, Nucleation site density in forced-convection boiling, J. Heat Transfer 115 (1993) 215–221.
[10] C.H. Wang, V.K. Dhir, Effect of surface wettability on active nucleation site density during pool boiling of water on a vertical surface, J. Heat Transfer 115 (1993) 659–669.
[11] C.H. Wang, V.K. Dhir, On the gas entrapment and nucleation site density during pool boiling of saturated water, J. Heat Transfer 115 (1993) 670–679.
[12] R.J. Benjamin, A.R. Balakrishnan, Nucleation site density in pool boiling of saturated pure liquids: effect of surface microroughness and surface and liquid physical properties, Exp. Thermal Fluid Sci. 15 (1997) 32–42.
[13] R.J. Benjamin, A.R. Balakrishnan, Nucleation site density in pool boiling of binary mixtures: effect of surface microroughness and surface and liquid physical properties, Can. J. Chem. Eng. 75 (1997) 1080–1089.
[14] S.R. Yang, Z.M. Xu, J.W. Wang, X.T. Zhao, On the fractal description of active nucleation site density for pool boiling, Int. J. Heat Mass Transfer 44 (2001) 2783–2786.
[15] N. Basu, G.R. Warrier, V.K. Dhir, Onset of nucleate boiling and active nucleation site density during subcooled flow boiling, J. Heat Transfer 124 (2002) 717–728.
[16] S.G. Bankoff, Entrapment of gas in the spreading of a liquid over a rough surface, AIChE J. 4 (1958) 24–26.

[17] J.J. Lorenz, The effects of surface conditions on boiling characteristics, Ph.D. Thesis, Massachusetts Institute of Technology, Cambridge, MA, USA, 1971.
[18] P. Griffith, J.D. Wallis, The Role of Surface Conditions in Nucleate Boiling, Chemical Engineering Progress Symposium Series, no. 30, vol. 56, 1960, pp. 49–63.
[19] V. Borishanskii, G. Bobrovich, F. Minchenko, Heat transfer from a tube to water and to ethanol in nucleate pool boiling, in: S.S. Kutateladze (Ed.), Symposium of Heat Transfer and Hydraulics in Two-Phase Media, Gosenergoizdat, Moscow, 1961.
[20] J.D. Bernardin, I. Mudawar, C.B. Walsh, E.I. Franses, Contact angle temperature dependence for water droplets on practical aluminum surfaces, Int. J. Heat Mass Transfer 40 (1997) 1017–1033.
[21] S.G. Kandlikar, M.E. Steinke, Contact angles and interface behavior during rapid evaporation of liquid on a heated surface, Int. J. Heat Mass Transfer 45 (2002) 3771–3780.
[22] A.E. Bergles, W.M. Rohsenow, The determination of forced-convection surface-boiling heat transfer, J. Heat Transfer 1 (1964) 365–372.